journal of the mechanical behavior of biomedical materials 104 (2020) 103701

Contents lists available at ScienceDirect

Journal of the Mechanical Behavior of Biomedical Materials

journal homepage: http://www.elsevier.com/locate/jmbbm

Mechanical behaviour of composite calcium phosphate–titanium cranial implants: Effects of loading rate and design

Susanne Lewin [a,*], Jonas Åberg [a], Dominique Neuhaus [b], Håkan Engqvist [a], Stephen J. Ferguson [b], Caroline Öhman-Mägi [a], Benedikt Helgason [b], Cecilia Persson [a]

[a] Div. of Applied Materials Science, Dept. of Engineering Sciences, Uppsala University, Uppsala, Sweden
[b] Institute for Biomechanics, ETH Zurich, Zurich, Switzerland

ARTICLE INFO

Keywords:
Cranial implants
Drop-tower
Bioceramics
Impact
Monetite
Ti4Al6V

ABSTRACT

Cranial implants are used to repair bone defects following neurosurgery or trauma. At present, there is a lack of data on their mechanical response, particularly in impact loading. The aim of the present study was to assess the mechanical response of a recently developed composite calcium phosphate–titanium (CaP–Ti) implant at quasi-static and impact loading rates.

Two different designs were tested, referred to as Design 1 (D1) and Design 2 (D2). The titanium structures in the implant specimens were additively manufactured by a powder-bed fusion process and subsequently embedded in a self-setting CaP material. D1 was conceptually representative of the clinically used implants. In D2, the titanium structure was simplified in terms of geometry in order to facilitate the manufacturing. The mechanical response of the implants was evaluated in quasi-static compression, and in impact using a drop-tower.

Similar peak loads were obtained for the two designs, at the two loading rates: 808 ± 29 N and 852 ± 34 for D1, and 840 ± 40 N and 814 ± 13 for D2. A strain rate dependency was demonstrated for both designs, with a higher stiffness in the impact test. Furthermore, the titanium in the implant fractured in the quasi-static test (to failure) but not in the impact test (to 5.75 J) for D1. For D2, the displacement at peak load was significantly lower in the impact test than in the quasi-static test. The main difference between the designs was seen in the quasi-static test results where the deformation zones, i.e. notches in the titanium structure between the CaP tiles, in D1 likely resulted in a localization of the deformation, compared to in D2 (which did not have deformation zones). In the impact test, the only significant difference between the designs was a higher maximum displacement of D2 than of D1. In comparison with other reported mechanical tests on osteoconductive ceramic-based cranial implants, the CaP–Ti implant demonstrates the highest reported strength in quasi-static compression. In conclusion, the titanium structure seems to make the CaP–Ti implant capable of cerebral protection in impact situations like the one tested in this study.

1. Introduction

Following neurosurgery or trauma, cranial defects can be repaired in a cranioplasty by using autologous bone or synthetic implants. The purpose of cranioplasty is to provide cerebral protection, restore aesthetics and relieve neurological symptoms (Neovius and Engstrand, 2010), (van de Vijfeijken et al., 2018). However, the reported complication rates for cranioplasty are high (~20%). Extensive bone resorption is the most common complication when using autologous bone in cranioplasty. However, infections are common for both autologous bone and synthetic implants (van de Vijfeijken et al., 2018). A variety of synthetic implant materials have been used, the most common ones being poly(methyl methacrylate) (PMMA), titanium based alloys, hydroxyapatite (HA) and polyether ether ketone (PEEK) (van de Vijfeijken et al., 2018). All these materials have different advantages and limitations in terms of mechanical properties, biocompatibility and potential for osseointegration. Yet, there is no consensus regarding the optimal solution (Zanotti et al., 2016). In order to understand differences in performance of available treatment options, cranial implants need to be studied in simulated real-life scenarios relevant for their application. As

* Corresponding author. Div. of Applied Materials Science, Department of Engineering Sciences Uppsala University, Box 534, 751 21, Uppsala, Sweden.
E-mail address: susanne.lewin@angstrom.uu.se (S. Lewin).

https://doi.org/10.1016/j.jmbbm.2020.103701
Received 14 December 2019; Received in revised form 4 February 2020; Accepted 13 February 2020
Available online 15 February 2020

one of the most critical functions of the cranium is cerebral protection, the mechanical behaviour of cranial implants is of high importance (Yoganandan et al., 1995).

Since there is no continuous loading to the skull, cranial implants are regulated as non-load bearing implants. Therefore, mechanical investigations are rare and no standardized mechanical test methods are available for these implants. Most reported studies have tested the implants in quasi-static compression using an indenter, but the low number of studies and setup differences in previous mechanical tests (e.g. specimen geometry, indenter shape, deformation rate) complicate inter-study comparison (Berretta et al., 2018; El Halabi et al., 2011; Lethaus et al., 2011; Matic and Manson, 2004; Ono et al., 1998; Piitulainen et al., 2017; Stefini et al., 2015; Ambrogio et al., 2018). However, impact loading is probably the most realistic loading scenario but potentially also the most destructive. To the authors' knowledge, this type of loading has only been investigated for cranial implants in two previous experimental studies (Matic and Manson, 2004), (Ambrogio et al., 2018). Furthermore, no previous study has conducted both quasi-static and impact tests.

Cranial implants have commonly been constructed from inert materials such as titanium alloys or PMMA. An improved outcome could potentially be obtained through a use of bioactive and osteoconductive materials, which offer better osseointegration and vascularization at the defect site, and may lower the infection rate (Engstrand, 2012). Recently, implants from this type of materials have been introduced clinically as bioactive glass fiber–reinforced composites or calcium phosphate-based implants (Stefini et al., 2013; Piitulainen et al., 2015; Kihlström Burenstam Linder et al., 2019; Lindner et al., 2017). Among these, sintered HA implants have seen the widest clinical use. However, fracture rates between 0 and 21% have been reported for HA implants in clinical studies, with some fractures occurring during insertion or even without reported trauma (Lindner et al., 2017; Moleset al., 2018; Zanotti et al., 2015). Fractures have previously been reported for PMMA or titanium mesh-type cranial implants, but only in case studies (Ko et al., 2014; van de Vijfeijken et al., 2019; Jiang et al., 2016). Consequently, the mechanical evaluation of newly introduced cranial implants is important.

The present study focuses on a patient-specific titanium-reinforced calcium phosphate (CaP–Ti) implant, which has shown promising clinical results (Kihlström Burenstam Linder et al., 2019; Engstrand et al., 2014; Sundblom et al., 2018; Engstrand et al., 2015). In a recent retrospective study of 50 patients, 5.7% developed complications which lead to implant removal. The outcome was promising, as this patient cohort previously had a 64% failure rate with autologous bone or other synthetic implants (Kihlström Burenstam Linder et al., 2019). In comparison with other inert materials, the calcium phosphate (CaP) material may provide improved biocompatibility, osseointegration and osteoconduction. However, all CaP materials are inherently brittle (Ajaxon et al., 2017), (Ajaxon et al., 2017), a titanium structure adds structural support in the CaP–Ti implant. As the positive clinical results could increase the clinical use of the CaP–Ti implant, a scientific investigation of the protective capability of the implant is necessary. Quasi-static mechanical testing has been performed on these implants ahead of clearance by regulatory authorities ('OssDsign 510 (K161090)'., 1610), and in a clinical study for comparison with another implant type (Kihlström Burenstam Linder et al., 2019). However, the scientific publication is limited to one quasi-statically tested specimen.

Moreover, at least two other factors make further mechanical evaluation of the CaP–Ti implants particularly interesting. Firstly, the design of the titanium structure contains small notches (deformation zones) intended to allow for controlled deformation in the titanium between the CaP tiles. They can most likely guide failure to predetermined locations but may decrease the overall stiffness and strength of the structure. It is important to investigate how these design features affect the implant performance at different loading rates. Secondly, the titanium structure of the implant is additively manufactured by a powder bed fusion-laser beam (L-PBF) process. In general, additive manufacturing of fine structures can be challenging. Complex geometries may also require additional post processing and support structures (DebRoy et al., 2019), (Conneret al., 2014). It would therefore be of interest to evaluate titanium structures with less complex design features that potentially facilitate production, and also improve time and cost effectiveness.

The aim of the present study was twofold; first, to assess the mechanical response of CaP–Ti cranial implants at quasi-static and impact loading rates in a biomechanically relevant test setup. Second, to assess the possibility of modifying the implant design for the purpose of facilitating production but preserving the implant strength. We hypothesized that the loading rate would significantly affect the maximum load that the implants could withstand. Furthermore, we hypothesized that the two implant designs would have similar mechanical strength.

2. Materials and methods

2.1. Design and manufacturing of implants

Cranial defects are commonly defined as large if the area is larger than 25 cm^2 (Neovius and Engstrand, 2010), (Durham et al., 2003). However, implant sizes and shapes vary greatly. In a recent review the sizes varied between 1.5 and 517 cm^2 (van de Vijfeijken et al., 2018). In our study, the implant specimens were designed in a generic shape with a circular geometry ($ø = 80$ mm). A circular shape was used in order to ensure reproducible results, with an area of ~50 cm^2 to ensure a definition as a large defect. The radius of the specimen curvature was set to 90 mm, which is in the range of measured skull curvatures (Laure et al., 2010).

CAD-geometries of two implant designs (Fig. 1) were created using commercial software (Rhinoceros 3D, release 5, Robert McNeel & Associates, USA). Design 1 (D1) was conceptually representative of implants that are used clinically (OSSDSIGN Cranial, OssDsign, Uppsala, Sweden). The main differences were the generic, rather than patient-specific geometry, and the absence of fixations. The rods in the titanium mesh structure had a rectangular cross-section of 0.6×1.6 mm^2. The CaP tiles were hexagonally shaped with a thickness of 6 mm – an average thickness for cranial bone (Moreira-Gonzalez et al., 2006). Between the tiles, deformation zones (0.3 mm notches) were placed (Fig. 1a). For the modified design (D2), the deformation zones in the titanium structure were removed. The cross-section of the rods was changed to circular with a diameter of, $ø = 1.2$ mm. This rod diameter was based on finite element simulations (static simulations using linear elastic material, data not shown), conducted to evaluate the amount of titanium required to maintain the strength in D2 compared to D1. The middle CaP tile in D2 was circular, the other tiles were placed in a pattern surrounding the central tile (Fig. 1b). The size of the tiles was larger in D2 compared to D1, but the thickness was kept the same as in D1 (6 mm). As previously mentioned, the simplifications in the titanium structure in D2 were made to facilitate the additive manufacturing process. The less complex design in D2 requires less support structures and less post processing, making the manufacturing of D2 more effective in terms of time and cost.

Implant specimens with the current (D1, $n = 12$) and the modified design (D2, $n = 12$) were manufactured by L-PBF in a titanium alloy (Ti–6Al–4V). The CaP formulation in the implants consists of monetite (86%), β-tricalcium phosphate (7%) and β-calcium pyrophosphate (7%), with a final porosity of approximately 40% (Engstrand et al., 2014). All implant specimens were manufactured by OssDsign (OssDsign, Uppsala, Sweden).

2.2. Mechanical testing of implant specimens

A rigid hollow steel cylinder was used to support the specimens around the circumference during the mechanical testing. In the contact

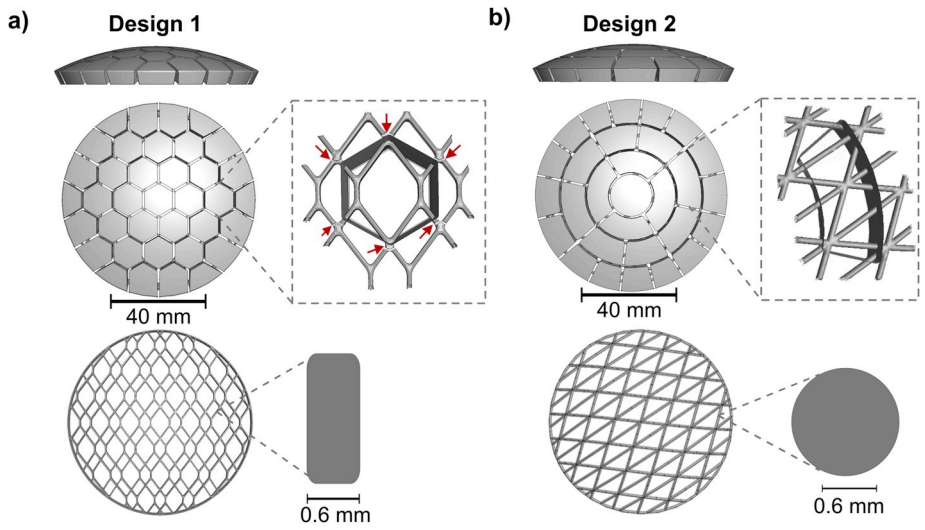

Fig. 1. Overview of D1 (a) and D2 (b). The CAD-geometries of the full implant designs are shown from the side and the top, together with the placement of the CaP tiles over the titanium. In D1, the placements of the deformation zones are marked by red arrows. The full titanium structures are shown in the bottom row for both implants, together with the cross-section of the titanium structures for each design: D1-rectangular (0.6×1.6 mm^2) and D2-circular ($\varnothing = 1.2$ mm).

between the support at the implant, the shape of the CaP tiles matched the inclined shape of the cylinder walls. As previous mechanical testing of CaP materials has demonstrated a significant difference in mechanical properties between wet and dry specimens (Ajaxon and Persson, 2017), the implants were kept at 37 °C in phosphate buffered saline (PBS, Sigma-Aldrich, pH = 7.4) for 24 h before testing. In order to obtain firm contact between ceramic tiles and the support, CaP cement was applied to the contact surface of the steel support. The cement set for 4 h in PBS at 37 °C prior to mechanical testing.

In previous impact tests, the presence of soft tissue had a significant damping effect when comparing the mechanical response of intact heads vs. isolated skulls (Verschueren et al., 2007) or synthetic head models with or without soft tissue (Trotta et al., 2018). One previous study used silicon rubber as a soft tissue surrogate in the mechanical testing of cranial implants (Stefini et al., 2015). To model soft tissue during our testing, a silicone rubber sheet with 5 mm thickness and 30 Shore A hardness (Microset 101 fluid, Microset Products Ltd, UK) was placed on top of the implants. The choice of silicone material and the thickness was based on previous literature (Falland-Cheung et al., 2015), (Young, 1959).

2.2.1. Quasi-static mechanical test

The support cylinder and implant specimen were placed in a universal test machine (AGS-X, Shimadzu Corp., Japan). A hemispherical indenter ($\varnothing = 40$ *mm*) was used to apply vertical compressive load to the centre of the implant (Fig. 2). The displacement during the test was measured with an optical encoder. In all tests the displacement data was corrected for machine compliance and zeroed at a load value of 3 N.

Initially, non-destructive testing was performed without the silicone sheet in order to obtain the implant stiffness; five preconditioning cycles from zero to 100 N were performed at a loading rate of 1 mm/min. From the last cycle, the implant stiffness was calculated from the linear part of the force vs. displacement curve, as the slope between 0.02 and 0.06 mm displacement. Subsequently, the silicone rubber sheet was placed on top of the implant and five preconditioning cycles at a loading rate of 1 mm/min were performed. Finally, the test to failure was conducted at the same loading rate. The full quasi-static test setup can be seen in Fig. 2. The point at which the first CaP fractured and the point of peak load were noted. The CaP fracture point was defined as the first point of a decrease in force. The peak load was defined as the maximum force measure in the test. The stiffness of the implant and silicone together, referred to as construct stiffness, was calculated as the slope between

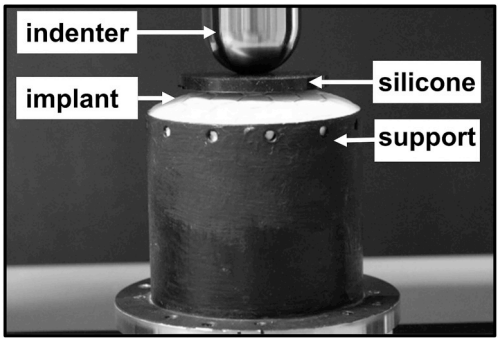

Fig. 2. An implant specimen and test setup before a quasi-static test.

1.5 mm and 3 mm displacement. Additionally, the energy absorption was calculated as the area under the force–displacement curves from zero to 15 mm displacement. For each group six specimens were tested in the quasi-static test. In the first test, however, a D1 specimen was not stable in the support, which prevented the test from being completed. Consequently, the amount of CaP cement on the support was increased in the protocol for the subsequent tests.

2.2.2. Impact test

A drop-tower rig was designed to measure the mechanical response of the implants at impact loading rates. A moving carriage was mounted on supporting columns with linear bearings to minimize friction. The weight of the drop-tower carriage was 5 kg, which is in the upper range of the mass of human heads (Yoganandan et al., 2009). A hemispherical indenter ($\varnothing = 40$ *mm*) was attached to the bottom of the carriage.

Previous literature on impact testing for cranial bone was reviewed in order to determine impact conditions. In a similar setup, intact cranial parietal bone was impacted by a pendulum hammer with a flat indenter ($\varnothing = 30$ *mm*) at different impact energies, until fracture occurred at on average 11.4 J (ranging from 5.6 J to 19.8 J) (Laure et al., 2010). Another study dropped heads, intact except for removal of the mandibles, at 4.5–10.2 J without fractures (drop height 15–30 cm, mass 3.08–3.45 kg) (Loyd et al., 2014). Based on these previous studies, the test was set up to represent a significant head impact which would likely not result in a skull fracture for average cranial bone. A target impact energy of $E_{impact} = 5.6\,J$ and an impact velocity of $v_{max} = 1.5\,m/s$ were

chosen with a corresponding drop-height of 0.115 m. Moreover, as damage in the CaP could be expected at this impact speed (Garcia--Gonzalez et al., 2017), the protective ability of the titanium beyond this point would be evaluated.

Using the same procedure as in the quasi-static tests, CaP cement was added onto the edges of the support before placing the implant specimen. The specimen with the silicone rubber sheet on top was then placed in the drop-tower (Fig. 3). A high-speed camera (IDT Y8–S2, Integrated Design Tools Inc., USA) was used to record the displacement during the impact tests. Images were obtained at a sampling rate of 6800 frames/second (FPS). The resolution of the images was 1600 × 1200 pixels. The images were used to track the displacement between two circular markers (ø = 10 mm). One marker was placed on the support and the other one on the carriage. Image processing was conducted in Matlab 9.6 (The MathWorks, USA), where the central positions of the markers were obtained for each frame.

A piezoelectric force sensor (208C04, PCB Piezotronics, Inc., USA), was placed between the indenter and the carriage (Fig. 3) (measurement range: 4.448 kN). The force sensor data was sampled at 13600 FPS, twice the sampling rate of the camera. The sensitivity was used to convert the voltage to force. A multifunction data acquisition (DAQ) device (NI USB-6210, National Instruments, Inc., USA) was used for data recording. The complete system was controlled by a software (LabVIEW, National Instruments, Inc., USA). In order to obtain a synchronized data output, a trigger system was installed in the form of a magnetic sensor, which was placed below the drop-height. A magnetic plate was placed on the carriage (Fig. 3). As the carriage passed the magnetic sensor, a signal was sent to a junction box that connected the trigger system to the DAQ.

From the primary impact force–displacement data, the construct stiffness was determined as the slope between 1.5 mm and 3 mm displacement. Additionally, peak load, displacement at peak load, and energy absorbed until peak load were calculated. From the displacement–time data, the actual impact velocity and the corresponding impact energy was obtained. Six specimens were tested for both D1 and D2. The displacement and time were adjusted to zero at the point where a force of at least 3 N was measured.

2.3. Statistical analysis

Statistical analysis was performed in R (version 3.5.2) (R Core Team, 2014). The analyses were conducted to assess differences among the designs and loading rates. First, Shapiro-Wilk and Levene's tests were conducted to assess the normality and the homoscedasticity of the data. Subsequently, a two-way ANOVA was conducted for construct stiffness, peak load and displacement at peak load to assess differences between designs and loading rates, i.e. having design and test type as factors. If the interaction was significant, a Tukey's post hoc test was performed between interactions.

For variables tested only for one loading rate between designs or vice versa, the results were compared by Welch two sample *t*-test. Statistically significant differences were confirmed for a probability value $p < 0.05$.

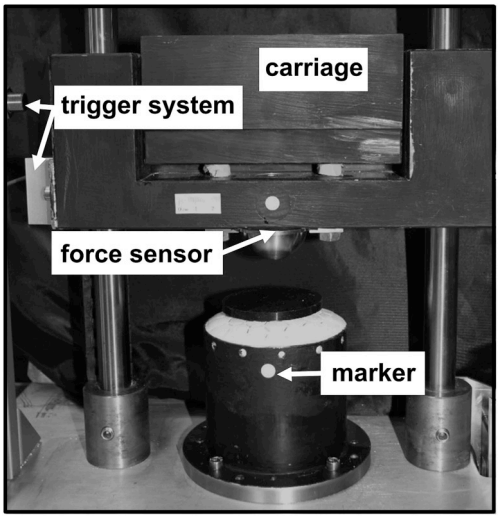

Fig. 3. The drop-tower setup and the implant specimen before an impact test. The positions of the different parts (trigger system, force sensor, marker and carriage) are marked in the image.

3. Results

3.1. Quasi-static mechanical test

Results from the quasi-static tests are listed in Table 1 and illustrated in Fig. 4. Overall, the quasi-static test setup provided repeatable results for both D1 and D2 specimens. The data was analysed before the force had dropped below 50% of the peak load (Table 1).

The force–displacement response for one representative specimen from each group are shown in Fig. 4a. All specimens had a similar nonlinear response until CaP fracture. Subsequently, the D1 specimens continued with a similar stiffness until fractures occurred in the titanium structure, around the peak load at 808 ± 29 N and 6.2 ± 0.7 mm. Post-test examination of these specimens showed that the titanium broke in the same manner in all specimens. First, in the deformation zones around the middle CaP tile directly below the indenter, and subsequently in the adjacent deformation zones. In Fig. 4b the ceramic has been removed from a D1 specimen, tested until 50% drop in peak force, to show the location of the fractures in the titanium structure.

In the force–displacement response of the D2 specimens, a plateauing force was seen around 5–10 mm displacement, referred to as peak 1. Peak 1 occurred at on average a displacement of 6.5 ± 0.1 mm, and a force of 671 ± 14 N. The force increased until peak load, at 846 ± 40 N and 11.7 ± 0.5 mm, and subsequently dropped to below 50% of the peak load. The testing of one D2 specimen was stopped at this force, just before 20 mm deformation, in order to investigate the deformation of the titanium structure. The post-test examination of this specimen showed no fractures in the titanium. However, the titanium structure was deformed to 18 mm. In Fig. 4c, most ceramic has been removed and this deformation can be observed. After removing all the ceramic, the titanium structure deformed back to its original shape (Fig. 4d). Displacements over ~20 mm caused instability at the support for D2 specimens, due to cracking at the edges of the CaP. The remaining D2 specimens were nevertheless tested beyond this point to study the fracture process of the titanium structures.

3.2. Impact test

Results for all specimens from the primary impacts can be found in Fig. 5a–d and Table 2. Overall, repeatable measurements were obtained for force vs. time (Fig. 5a) and displacement vs. time (Fig. 5b). The impact velocity and energy (1.52 m/s and 5.75 J; Fig. 5c) were not significantly different between designs, and corresponded well to the targeted impact velocity and energy (1.50 m/s and 5.6 J).

The force vs. displacement response from the impact test appeared similar and overlapping for D1 and D2 (Fig. 5d). Just as in the quasi-static test, D2 had two peaks. The peak force (maximum force) occurred at the second peak in the majority of D2 specimens (814 ± 13 N and 7.7 ± 2.6 mm), at a similar force and displacement as D1 (852 ± 34 N and 5.9 ± 1.0 mm). Peak 1 occurred at a similar force (798 ± 34 N), but at a lower displacement (5 ± 0.6 mm). It was not possible to distinguish the point of CaP fracture in the force vs. displacement data from the impact test. However, fractures in the CaP tiles were observed in all implants after testing. The central tile was the most severely

Table 1
Results from the quasi-static testing. The mean values and standard deviations are presented for the total number of specimens (n).

Specimen type	n	Implant stiffness[a] [N/mm]	Construct stiffness [N/mm]	CaP fracture [N]	Displacement at CaP fracture [mm]	Peak load[b] [N]	Displacement at peak load[b] [mm]	Energy absorbed at 15 mm [J]
D1	5	1632 ± 173	152 ± 20	463 ± 45	3.5 ± 0.1	808 ± 29	6.2 ± 0.7	7.3 ± 0.4
D2	6	1675 ± 156	156 ± 10	368 ± 18	3.2 ± 0.1	846 ± 40	11.7 ± 0.5	8.4 ± 0.1

[a] Until 100 N without silicone rubber (between 0.02 and 0.06 mm displacement).
[b] Before the force had dropped to 50% of the peak load.

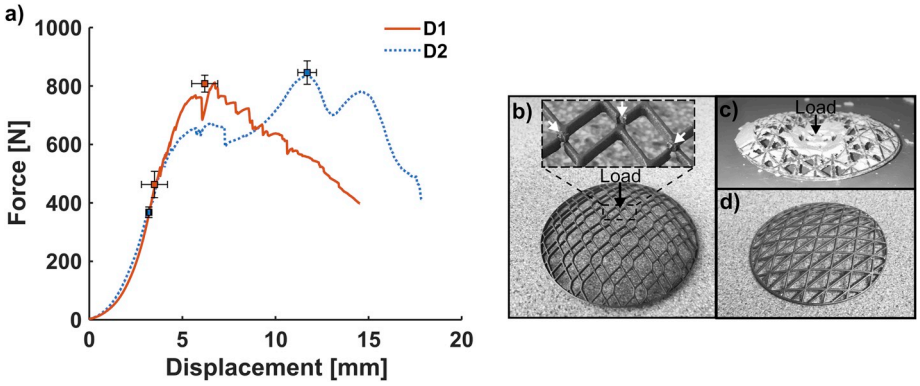

Fig. 4. Results from the quasi-static testing. The force–displacement response until 50% decrease in peak load (a), presented for one representative D1 (red solid line) and one representative D2 specimen (blue dotted line). The mean values of all specimens for load and displacement at the points of CaP fracture and peak load are marked (□) together with the standard deviations (error bars). Post-test images of the titanium structures with the CaP removed are shown in (b)–(d). In (b), a D1 specimen (load direction marked) with a magnification showing the fracture locations (white arrows). In (c), a deformed (load direction marked) D2 specimen directly after the test, and later after cleaning the titanium, when the structure recovered its shape (d). The two specimens derive from tests stopped at ~50% decrease in peak load.

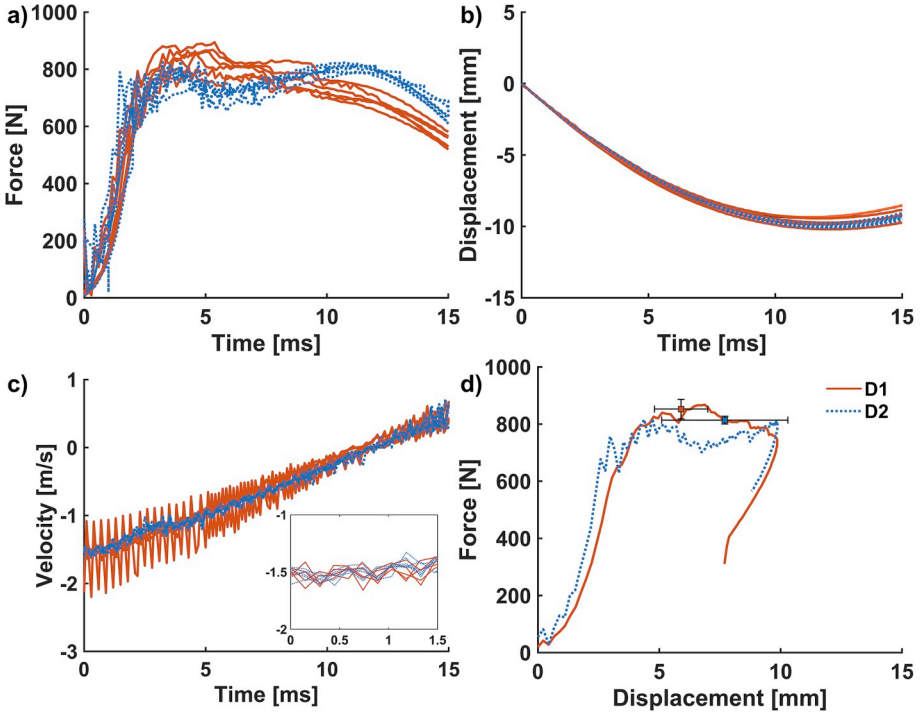

Fig. 5. Results from the impact test. Data from the primary impact is presented for D1 (red solid lines) and D2 (blue dotted lines). Impact force vs. time (a), displacement vs. time (b), and impact velocity vs. time (c). A zoomed in view is shown in the bottom right corner, one specimen was removed in the zoom due to large deviations in the data. In d) impact force vs. displacement is presented for one representative specimen from each group. The peak loads are marked in the graph (□) together with the standard deviations (error bars).

affected part of the implant and fractured fragments of this tile fell through the titanium structure. Some of the other tiles also fractured, but to a lesser extent in locations farther away from the impact point. When the implant had been removed from the support, it was observed that some of the CaP tiles on the bottom side of the implant had detached. Nevertheless, no titanium fractures were observed after testing in any of the designs, and the titanium structures retained their original shape.

3.3. Statistical comparisons between designs and loading rates

Two-way ANOVA was used for comparing construct stiffness, peak load and displacement at peak load between loading rates and designs (Fig. 6). The construct stiffness was not significantly different between the designs. The construct stiffness was, however, significantly higher at impact than at quasi-static loading rates, for both specimen types ($p < 0.001$). There was no significant difference in peak load. For displacement at peak load the interaction between design and loading rate was significant ($p < 0.01$). The post hoc test showed that D2 at the quasi-

Table 2
Results from the impact test. The mean values and standard deviations are presented for the total number of specimens (n).

Specimen type	n	Construct stiffness [N/mm]	Max displacement [mm]	Peak load [N]	Displacement at peak load [mm]	Energy absorbed at peak load [J]	Impact velocity [m/s]	Impact Energy [J]
D1	6	295 ± 53	9.4 ± 0.3	852 ± 34	5.9 ± 1.0	3.1 ± 0.8	1.52 ± 0.01	5.75 ± 0.09
D2	6	309 ± 53	10.0 ± 0.3	814 ± 13	7.7 ± 2.6	4.4 ± 1.8	1.52 ± 0.02	5.75 ± 0.1

static loading rate explain these significant results, since a significantly higher displacement at peak load was obtained, compared to the other tests or designs ($p < 0.001$). Similarly, the force and displacement at peak 1 for D2 was significantly different in a *t*-test comparing the loading rates ($p < 0.001$ and $p < 0.01$).

In the variables specific for the quasi-static test, CaP fractures were observed at a lower load ($p < 0.01$) and at a lower displacement ($p < 0.01$) for D2 compared to D1 specimen (Fig. 6). There was no significant difference in implant stiffness between designs. The energy absorbed at 15 mm was higher ($p < 0.001$) for D2 compared to D1 specimens. The point of 15 mm deformation was evaluated, as a depression of 10 mm typically requires surgical treatment (Seule et al., 2015), (Bullocket al., 2006), and a ~5 mm silicone deformation and compression of the CaP material could be assumed.

In the variables specific for the impact test, the maximum displacement was significantly higher for D2 compared to D1 ($p = 0.003$). However, the absolute difference (0.6 mm) was small. The energy observed at peak load was not significantly different between designs.

4. Discussion

The aim of this study was twofold. On the one hand, it aimed to compare the mechanical response of CaP–Ti cranial implants under quasi-static and impact loading conditions respectively. On the other, it aimed to compare two different implant designs under these loading conditions. For the variables compared between designs and loading rates, we found significant differences between the two designs in the quasi-static test. However, at impact loading rates, the behaviour of the two designs was more similar.

Comparing the two designs in the quasi-static tests, the first CaP fractures were observed at a significantly higher load for D1 compared to D2 specimens. The difference was small in absolute numbers ~100 N, but comparing the two designs the CaP fracture force was 20.5% lower for D2 compared to D1. This outcome could have relevance for understanding differences in the two designs in regards to the size of the ceramic tiles, and presence of the deformation zones. Ceramic materials such as CaP are generally sensitive to defects (e.g. pores and microcracks), as the occurrence of defects will increase with an increase in material volume (Danzer, 1992). The ceramic tiles in D2 were larger than in D1. In the quasi-static tests, the CaP-tiles started to fracture as the titanium structure deformed, due to their brittleness. The CaP in D2 fractured at a lower displacement than in D1, likely because of the deformation zones, which seem to guide the deformation to predetermined locations outside of the CaP tiles. Nevertheless, the absolute difference in displacement at CaP fracture was also small, 0.3 mm.

The differences in implant and construct stiffness between D1 and D2 were found not to be significant, independent of loading rate. In fact, the circular cross-section in D2 leads to a reduced bending stiffness, however the deformation zones reduced the stiffness in D1, which could explain the similarities in stiffness in the two designs. However, the design changes involved too many parameters (cross-sectional shape, removal of deformation zones, the shape and size of the tiles etc.) to establish whether a change in a certain feature (e.g. removal of deformation zones) on its own caused a different implant behaviour.

Other differences in mechanical response were observed in the comparison between the two designs and the loading rates. While the peak load was not significantly different, D2 reached peak load at a higher displacement than D1 in the quasi-static. Again, the deformation zones in D1 might explain this outcome. In the quasi-static test, the whole titanium structure deformed for D2, but only fractured after 20 mm deformation. In contrast, the D1 structure deformed more locally and fractured at peak load, ~6 mm deformation (Fig. 4). The deformation behaviour of D1 is likely clinically preferable. In the impact test the displacement at peak load was similar for the two designs. The difference in D2 between the tests indicates a load rate dependent bifurcation point in the deformation behaviour of D2. Overall, D1 had a more controlled deformation that depended less on the loading rate, potentially due to the deformation zones. To summarize the comparison of the

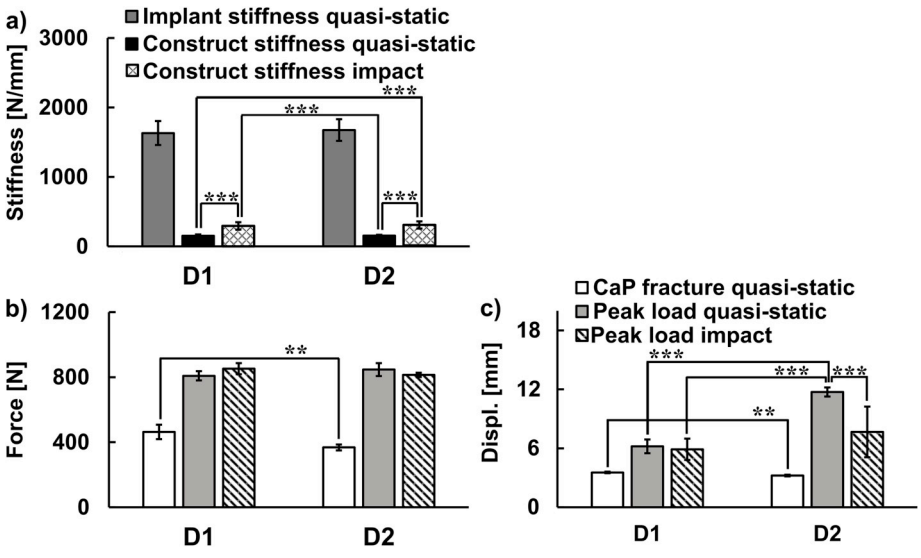

Fig. 6. Comparison of results for D1 and D2. The results from the quasi-static test (filled bars) and the primary impact in the drop-test (patterned bars) are presented. The implant stiffness (quasi-static) and construct stiffness (quasi-static and impact) are compared in a). The points of CaP fracture (quasi-static) and peak load (quasi-static and impact) from the force vs. displacement response are compared in b) and c). Here, b) shows the force and c) the displacement. Significant differences from the statistical tests are marked (** for $p \leq 0.01$, and *** for $p \leq 0.001$). The statistical tests were conducted between designs and loading rates for construct stiffness, peak load and displacement at peak load. For implant stiffness, CaP fracture load and CaP fracture displacement the tests were made between designs.

designs: D2 and D1 had differences in mechanical response in the quasi-static test. In the impact test, the mechanical behaviour of the two designs was more similar. However, since the impact loading rate creates a more realistic load case, D2 could be subjected to further evaluation. Since this design could facilitate the additive manufacturing of the titanium structure, such an evaluation would be of interest.

Effects of loading rate were observed although the peak force lacked significant differences for both loading rates and both designs. The construct stiffness was significantly higher in the impact compared to the quasi-static test for both designs. Moreover, in D1 the titanium fractured in the quasi-static test, but no fractures were observed in the titanium structure in D2. In the impact tests, the failures of the two designs were similar. The CaP tiles below the indenter fractured in all implants, but no fractures were observed in the titanium structures, with the implants retaining their shape.

Furthermore, the impact tests showed that although the CaP tiles could potentially fracture at impact, the titanium structure remained intact and capable of providing sufficient support for impacts of up to 5.75 J. The test aimed to produce a significant impact which potentially could occur in an everyday situation (e.g. hitting the head against a rigid

Table 3
Summary of mechanical test data on cranial implants. All included results concern tests made on curved implant specimen, which were supported on the outer edges.

Material category	Author	Materials tested	Clinically available product (company name)	Test specimens	Loading rate	Test conditions	Peak load
Ceramic	Ono et al. (1998)	Porous HA implants	Not found	**Implant size** Length: 113 mm Width: 63–75 mm **Implant thickness** 6 mm	Quasi-static: 0.5 mm/min	**Indenter** N/A **Support** N/A	165 N
Ceramic	Stefini et al. (2015)	Porous HA implants	Yes (Finceramica)	**Implant size** 66–100 cm^2 **Implant thickness** N/A	Quasi-static	**Indenter** Flat, ø = 25 mm **Support** Plaster powder, and epoxy adhesive **Soft tissue surrogate** Silicone rubber (25 Shore A)	726 ± 345 N
Composite	Piitulainen et al. (2017)	Glass fiber-reinforced composite with bioactive glass	Yes (Skulle Implants)	**Implant size** 112 × 67 mm **Implant thickness** 2.5 mm	Quasi-static: 1 mm/min	**Indenter** Flat, rectangular 17 × 55 mm **Support** Aluminium and screws	175 ± 101 N[b]
Composite	This study	Calcium phosphate (monetite based) and Ti–6Al–4V (L-PBF)	Yes (OssDsign)	**Implant size** ø = 80 mm **Implant thickness** ~6 mm	Quasi-static: 1 mm/min Impact: 1.52 m/s (5.75 J)	**Indenter** Hemispherical, ø = 40 mm **Support** Stainless steel and bone cement **Soft tissue surrogate** 5 mm silicone rubber (30 Shore A)	Quasi-static: 808 ± 29 N Impact: 846 ± 40 N
Polymer	Berretta et al. (2018)	PEEK, mesh-type implant	No (material available: PEEK Optima)	**Implant size** ~100 × 200 mm[a] **Implant thickness** N/A	Quasi-static: 1 mm/min	**Indenter** Hemispherical, ø = 10 mm **Support** Polymer and adhesive	794 N
Polymer	El Halabi et al. (2011)	PEEK, mesh-type implant	No (material available: PEEK Optima)	**Implant size** ~100 × 200 mm[a] **Implant thickness** N/A	Quasi-static: 0.1 mm/min	**Indenter** Hemispherical, ø = 10 mm **Support** Polyamide and screws	Implant 1: 608 ± 44 N Implant 2: 1028 ± 69 N
Polymer	Lethaus et al. (2011)	PEEK, solid implant	No (material available: PEEK Optima)	**Implant size** 100 cm^2 **Implant thickness** 6 mm	Quasi-static: 1.9 mm/min	**Indenter** Flat, ø = 10 mm **Support** Polyamide and screws	24 kN
Metal	Lethaus et al. (2011)	Ti–6Al–4V	No	**Implant size** 100 cm^2 **Implant thickness** 6 mm	Quasi-static: 1.9 mm/min	**Indenter** Flat, ø = 10 mm **Support** Polyamide and screws	50 kN[c]
Metal	Ambrogio et al. (2018)	Ti–6Al–4V (sheet-forming)	No	**Implant size** 100 cm^2 **Implant thickness** 1–1.5 mm	Impact: 4.5 J and 13.5 J	**Indenter** Hemispherical, ø = 20 mm **Support** PMMA and screws	1.4–4.7 kN

[a] Estimated from photographs.
[b] The test was run to 10 mm displacement but the force was evaluated at 6 mm displacement.
[c] The test was stopped due to damage in the support

corner), but would be unlikely to cause fracture in cranial parietal bone of average strength. In a similar test setup, using a pendulum hammer with a flat indenter ($\varnothing = 30$ *mm*), intact cranial parietal bone fractured on average at 11.4 J, in a range from 5.6 J to 19.8 J (Laure et al., 2010). Since the titanium structure in the CaP–Ti implant did not fracture from a 5.75 J impact, our testing could indicate that the titanium structure in both implant designs are at least as strong as the lower range of parietal bone. However, differences in test setups (mass, size and shape of indenter, velocity etc.) make this comparison less certain. The impact in our test could be more severe e.g. since a hemispherical indenter concentrates the force more than a flat one – nevertheless the size of the indenters was similar.

An overview of the literature for mechanical studies conducted on cranial implants can be found in Table 3 together with details of the test setups. Most implants were tested in a manner similar to the quasi-static test in this study (Berretta et al., 2018; El Halabi et al., 2011; Lethaus et al., 2011; Ono et al., 1998; Piitulainen et al., 2017; Stefini et al., 2015). In one study, porous HA implants failed at a peak load of 165 N (Ono et al., 1998). Another type of porous HA implants was tested covered by silicone rubber, and a peak load of 726 ± 345 N was measured (Stefini et al., 2015). Glass fibre-reinforced composite implants were tested by Piitulainen et al. (2017): the forces were evaluated at 6 mm displacement as 175 ± 101 N, the effect of bone ingrowth was then added which increased this value (Piitulainen et al., 2017). Compared to these results for HA and glass fibre-reinforced composite implants, our results show that the CaP–Ti implants likely provide additional mechanical support. Nonetheless, all these implant materials, including the CaP–Ti composite, have a potential for osteoconduction/osseointegration, which could improve their long-term mechanical support *in vivo*. As for studies on implants made from inert materials, two studies performed quasi-static testing of additively manufactured porous PEEK implants (mesh-type). Depending on implant design and manufacturing parameters, peak loads around 600–1000 N were measured (Berretta et al., 2018), (El Halabi et al., 2011). A solid PEEK implant was tested to failure at a load of 24 kN (Lethaus et al., 2011). In the same study, a solid titanium implant was tested. No damage was observed in the implant but in the support, and the test was stopped at 50 kN (Lethaus et al., 2011). However, the solid titanium implant was considerably thicker (6 mm) than those employed in typical clinical use (1–2 mm plate or mesh-type). These solid implants demonstrated very high strength and stiffness compared to the previously mentioned bioactive and mesh-type implants. In an impact, the high stiffnesses could nevertheless result in high load transfer from the implant to the bone interface, which could result in damage in the surrounding bone. Moreover, the cranial bone in an intact human cadaveric head would probably fracture from loads below those of the inert materials (~5 kN) (Yoganandan et al., 1995). Hence, implant designs which absorb the energy of an impact through controlled deformation may provide mechanical protection with a reduced risk of damaging the surrounding bone. Nonetheless, the ultimate protection of the brain with regard to overall deformation and penetration have to be considered as the most important function of a cranial implant.

Two experimental studies have tested cranial implants in impact loading (Matic and Manson, 2004), (Ambrogio et al., 2018). One study reconstructed defects in cadaver heads with HA cement and titanium mesh, and performed impact testing (Matic and Manson, 2004). However, the surrounding bone most likely absorbed energy in the impact, since the defect area (9 cm^2) was small compared to the indenter area (79 cm^2). This complicates evaluation of their implant system. Another study investigated titanium cranial implants at impact loading using a drop-tower setup (Ambrogio et al., 2018). The implants (thickness 1–1.5 mm) were manufactured using Ti–6Al–4V by a sheet-forming process (the curvature and shape were based on cranial anatomy). A hemispherical indenter was used for impacts of 4.5 J and 13.5 J. No implants fractured during the tests. Maximum deflection ranged from 1.9 to 9.7 mm, and peak loads from 1.4 to 4.7 kN, depending on impact energy, implant thickness and manufacturing parameters (Ambrogio et al., 2018). The maximum load at the 4.5 J impact was higher than in our tests. The maximum deflection in our test was 9.4 mm, but the deflection of the titanium structure was likely less since the silicone was 5 mm thick and the upper part of the CaP tiles was ~2 mm. Since the titanium did not fracture in any of the impact tests, it is difficult to make more specific statements about the ultimate strength of the CaP–Ti implants in relation to the titanium sheet-formed implants. In summary, considering the mechanical data available in the literature, comparisons would be facilitated if standardized mechanical tests for cranial implants were agreed upon. In such standardized tests, it would be important to have well defined failure criteria.

On the topic of failure, fractures in solid implants from brittle materials (e.g. PMMA or HA) could result in large fragments of sharp material (Moles et al., 2018; Zanotti et al., 2015; Ko et al., 2014; van de Vijfeijken et al., 2019). In one clinical case a fractured PMMA implant resulted in brain trauma for one patient (Ko et al., 2014). It should be beneficial to manufacture the brittle CaP material in smaller parts, as in the CaP–Ti implant. If an implant would be exposed to high impact loads, the fractured fragments of CaP material would not be larger than the size of one tile. Fragments would likely also be kept in place by surrounding bone and/or soft tissue (Kihlström Burenstam Linder et al., 2019). Additionally, fragments of the monetite based CaP material could degrade with time, either by dissolution or cell mediated degradation (Montazerolghaem et al., 2015), (Tamimi et al., 2010).

Limitations of the study include the simplification of the test setup in terms of biofidelity. In a real-life impact, additional soft tissues (scalp, dura mater, brain etc.) would likely provide additional damping. Furthermore, if the CaP tiles would fracture, they would likely be contained by soft tissue, and with time bone would also form around the CaP tiles (Kihlström Burenstam Linder et al., 2019), (Engstrand et al., 2015). A drop-tower impact test setup was chosen in order to obtain repeatable loading with controlled boundary conditions, which would facilitate validation of future computational models. However, this loading differs from the real-life impact as the implants are constrained by a rigid support. In an *in vivo* impact, a human head would be less constrained, and the implant would therefore experience a different load distribution (Verschueren et al., 2007). The implant-to-bone attachment is also different *in vivo*, since the implant typically is fixed to the cranial bone by screws. Nevertheless, the test setup offered a repeatable evaluation of the impact resistance of the implants, with controlled boundary conditions.

5. Conclusions

The mechanical behaviour of the two CaP–Ti implant designs was similar at the impact loading rate, which should be considered the most realistic loading. However, at quasi-static loading rates, the deformation zones seem to be important for the localization of the deformation and failure. A review of the available literature showed that the CaP–Ti implants demonstrated a higher strength in quasi-static compression when compared to other bioactive and osteoconductive ceramic-based cranial implants. Although the CaP tiles fractured in the impact test, the titanium structures remained intact and the implant shape was furthermore retained. In conclusion, the titanium structure seems to make the CaP–Ti implant capable of cerebral protection in impact situations like the one tested in this study.

Declaration of competing interest

The authors declare the following financial interests/personal relationships which may be considered as potential competing interests: Dr. Aberg and Prof. Engqvist have consulting agreements with OssDsign and also direct ownership in OssDsign. Prof. Engqvist is also on the board of OssDsign.

CRediT authorship contribution statement

Susanne Lewin: Investigation, Visualization, Methodology, Writing - original draft, Writing - review & editing. **Jonas Åberg:** Conceptualization, Methodology, Writing - review & editing. **Dominique Neuhaus:** Methodology, Writing - review & editing. **Håkan Engqvist:** Conceptualization, Funding acquisition, Writing - review & editing. **Stephen J. Ferguson:** Conceptualization, Funding acquisition, Writing - review & editing. **Caroline Öhman-Mägi:** Supervision, Writing - review & editing. **Benedikt Helgason:** Methodology, Supervision, Writing - review & editing. **Cecilia Persson:** Conceptualization, Methodology, Writing - review & editing, Supervision, Funding acquisition.

Acknowledgements

The authors gratefully acknowledge Johan Persson for assistance with developing the drop-tower setup, Alejandro López and Magnus Heldin for support during tests, and Ingmar Fleps for discussions. Funding from the Eurostars-2 Joint European Union's Horizon 2020 (project ID: E19741) is acknowledged.

References

Ajaxon, I., Persson, C., 2017. Mechanical properties of brushite calcium phosphate cements. In: The World Scientific Encyclopedia of Nanomedicine and Bioengineering II, vol. 9. WORLD SCIENTIFIC, pp. 285–300, 3 vols.

Ajaxon, I., et al., 2017. Elastic properties and strain-to-crack-initiation of calcium phosphate bone cements: revelations of a high-resolution measurement technique. J. Mech. Behav. Biomed. Mater. 74, 428–437. https://doi.org/10.1016/j.jmbbm.2017.06.023.

Ambrogio, G., et al., 2018. Experimental investigation of the mechanical performances of titanium cranial prostheses manufactured by super plastic forming and single-point incremental forming. Int. J. Adv. Manuf. Technol. 98 (5–8), 1489–1503.

Berretta, S., Evans, K., Ghita, O., 2018. Additive manufacture of PEEK cranial implants: manufacturing considerations versus accuracy and mechanical performance. Mater. Des. 139, 141–152.

Bullock, M.R., et al., Mar. 2006. Surgical management of depressed cranial fractures'. Neurosurgery 58 (Suppl. ment). https://doi.org/10.1227/01.NEU.0000210367.14043.0E pp. S2-56-S2-60.

Conner, B.P., et al., 2014. Making sense of 3-D printing: creating a map of additive manufacturing products and services. Addit. Manuf. 1, 64–76.

Danzer, R., Jan. 1992. A general strength distribution function for brittle materials. J. Eur. Ceram. Soc. 10 (6), 461–472. https://doi.org/10.1016/0955-2219(92)90021-5.

DebRoy, T., et al., 2019. Scientific, technological and economic issues in metal printing and their solutions. Nat. Mater. 1.

Durham, S.R., McComb, J.G., Levy, M.L., 2003. Correction of large (> 25 cm2) cranial defects with "reinforced" hydroxyapatite cement: technique and complications. Neurosurgery 52 (4), 842–845.

El Halabi, F., Rodriguez, J.F., Rebolledo, L., Hurtos, E., Doblaré, M., 2011. Mechanical characterization and numerical simulation of polyether–ether–ketone (PEEK) cranial implants. J. Mech. Behav. Biomed. Mater. 4 (8), 1819–1832.

Engstrand, T., 2012. Biomaterials and biologics in craniofacial reconstruction. J. Craniofac. Surg. 23 (1), 239–242.

Engstrand, T., Kihlström, L., Lundgren, K., Trobos, M., Engqvist, H., Thomsen, P., Aug. 2015. Bioceramic implant induces bone healing of cranial defects. Plast. Reconstr. Surg. Glob. Open 3 (8). https://doi.org/10.1097/GOX.0000000000000467.

Engstrand, T., et al., 2014. Development of a bioactive implant for repair and potential healing of cranial defects. J. Neurosurg. 120 (1), 273–277.

Falland-Cheung, L., Pittar, N., Tong, D., Waddell, J.N., Dec. 2015. Investigation of dental materials as skin simulants for forensic skin/skull/brain model impact testing. Forensic Sci. Med. Pathol. 11 (4), 552–557. https://doi.org/10.1007/s12024-015-9718-0.

Garcia-Gonzalez, D., et al., May 2017. On the mechanical behaviour of PEEK and HA cranial implants under impact loading. J. Mech. Behav. Biomed. Mater. 69, 342–354. https://doi.org/10.1016/j.jmbbm.2017.01.012.

Jiang, Y., Wang, Y.-K., Yu, M.-K., Jan. 2016. Spontaneous fracture of cranioplastic titanium implants without head trauma in an adult: a case report. Int. J. Surg. Case Rep. 24, 50–53. https://doi.org/10.1016/j.ijscr.2016.04.039.

Kihlström Burenstam Linder, L., Birgersson, U., Lundgren, K., Illies, C., Engstrand, T., Feb. 2019. Patient-specific titanium-reinforced calcium phosphate implant for the repair and healing of complex cranial defects. World Neurosurg. 122, e399–e407. https://doi.org/10.1016/j.wneu.2018.10.061.

Ko, A.L., Nerva, J.D., Chang, J.J.J., Chesnut, R.M., Oct. 2014. Traumatic fracture of a polymethyl methacrylate patient-specific cranioplasty implant. World Neurosurg. 82 (3–4), 536. https://doi.org/10.1016/j.wneu.2013.09.025 e11–13.

Laure, B., Tranquart, F., Geais, L., Goga, D., 2010. Evaluation of skull strength following parietal bone graft harvest. Plast. Reconstr. Surg. 126 (5), 1492–1499.

Lethaus, B., et al., Oct. 2011. Cranioplasty with customized titanium and PEEK implants in a mechanical stress model. J. Neurotrauma 29 (6), 1077–1083. https://doi.org/10.1089/neu.2011.1794.

Lindner, D., Schlothofer-Schumann, K., Kern, B.-C., Marx, O., Müns, A., Meixensberger, J., Jan. 2017. Cranioplasty using custom-made hydroxyapatite versus titanium: a randomized clinical trial. J. Neurosurg. 126 (1), 175–183. https://doi.org/10.3171/2015.10.JNS151245.

Loyd, A.M., Nightingale, R.W., Song, Y., Luck, J.F., Cutcliffe, H., Myers, B.S., 2014. The response of the adult and ATD heads to impacts onto a rigid surface. Accid. Anal. Prev. 72, 219–229.

Matic, D.B., Manson, P.N., 2004. Biomechanical analysis of hydroxyapatite cement cranioplasty. J. Craniofac. Surg. 15 (3), 415–422.

Moles, A., et al., Mar. 2018. Long-term follow-up comparative study of hydroxyapatite and autologous cranioplasties: complications, cosmetic results, osseointegration. World Neurosurg. 111, e395–e402. https://doi.org/10.1016/j.wneu.2017.12.082.

Montazerolghaem, M., Karlsson Ott, M., Engqvist, H., Melhus, H., Rasmusson, A.J., Jul. 2015. Resorption of monetite calcium phosphate cement by mouse bone marrow derived osteoclasts. Mater. Sci. Eng. C 52, 212–218. https://doi.org/10.1016/j.msec.2015.03.038.

Moreira-Gonzalez, A., Papay, F.E., Zins, J.E., 2006. Calvarial thickness and its relation to cranial bone harvest. Plast. Reconstr. Surg. 117 (6), 1964–1971.

Neovius, E., Engstrand, T., Oct. 2010. Craniofacial reconstruction with bone and biomaterials: review over the last 11 years. J. Plast. Reconstr. Aesthetic Surg. 63 (10), 1615–1623. https://doi.org/10.1016/j.bjps.2009.06.003.

Ono, I., Tateshita, T., Nakajima, T., Ogawa, T., 1998. Determinations of strength of synthetic hydroxyapatite ceramic implants. Plast. Reconstr. Surg. 102 (3), 807–813.

Piitulainen, J.M., Kauko, T., Aitasalo, K.M.J., Vuorinen, V., Vallittu, P.K., Posti, J.P., May 2015. Outcomes of cranioplasty with synthetic materials and autologous bone grafts. World Neurosurg. 83 (5), 708–714. https://doi.org/10.1016/j.wneu.2015.01.014.

Piitulainen, J.M., Mattila, R., Moritz, N., Vallittu, P.K., Jan. 2017. Load-bearing capacity and fracture behavior of glass fiber-reinforced composite cranioplasty implants. J. Appl. Biomater. Funct. Mater. 15 (4), e356–e361. https://doi.org/10.5301/jabfm.5000375.

R Core Team, 2014. R: A Language and Environment for Statistical Computing. R Foundation for Statistical Computing, Vienna, Austria. http://www.R-project.org/.

Seule, M., Brunner, T., Mack, A., Hildebrandt, G., Fournier, J.-Y., Aug. 2015. Neurosurgical and intensive care management of traumatic brain injury. Facial Plast. Surg. 31 (4), 325–331. https://doi.org/10.1055/s-0035-1562884.

Stefini, R., Esposito, G., Zanotti, B., Iaccarino, C., Fontanella, M.M., Servadei, F., 2013. Use of "custom made" porous hydroxyapatite implants for cranioplasty: postoperative analysis of complications in 1549 patients. Surg. Neurol. Int. 4.

Stefini, R., et al., 2015. The efficacy of custom-made porous hydroxyapatite prostheses for cranioplasty: evaluation of postmarketing data on 2697 patients. J. Appl. Biomater. Funct. Mater. 13 (2), 136–144.

Sundblom, J., Nowinski, D., Casar-Borota, O., Ryttlefors, M., Sep. 2018. Removal of giant intraosseous meningioma followed by cranioplasty using a custom-made bioceramic implant: case report. J. Neurosurg. 1–5. https://doi.org/10.3171/2018.4.JNS1850.

Tamimi, F., Torres, J., Bassett, D., Barralet, J., Cabarcos, E.L., 2010. Resorption of monetite granules in alveolar bone defects in human patients. Biomaterials 31 (10), 2762–2769.

Trotta, A., Zouzias, D., De Bruyne, G., Ní Annaidh, A., Jun. 2018. The importance of the scalp in head impact kinematics. Ann. Biomed. Eng. 46 (6), 831–840. https://doi.org/10.1007/s10439-018-2003-0.

van de Vijfeijken, S.E.C.M., et al., Sep. 2018. Autologous bone is inferior to alloplastic cranioplasties: safety of autograft and allograft materials for cranioplasties, a systematic review. World Neurosurg. 117, 443–452. https://doi.org/10.1016/j.wneu.2018.05.193 e8.

van de Vijfeijken, S.E.C.M., et al., Mar. 2019. Properties of an in vivo fractured poly (methyl methacrylate) cranioplasty after 15 years. World Neurosurg. 123, e60–e68. https://doi.org/10.1016/j.wneu.2018.11.026.

Verschueren, P., et al., Jan. 2007. A new test set-up for skull fracture characterisation. J. Biomech. 40 (15), 3389–3396. https://doi.org/10.1016/j.jbiomech.2007.05.018.

Yoganandan, N., Pintar, F.A., Zhang, J., Baisden, J.L., 2009. Physical properties of the human head: mass, center of gravity and moment of inertia. J. Biomech. 42 (9), 1177–1192.

Yoganandan, N., et al., Aug. 1995. Biomechanics of skull fracture. J. Neurotrauma 12 (4), 659–668. https://doi.org/10.1089/neu.1995.12.659.

Young, R.W., 1959. Age changes in the thickness of the scalp in white males. Hum. Biol. 31 (1), 74–79.

Zanotti, B., Verlicchi, A., Indiani, S., Scarparo, S.A., Zingaretti, N., Parodi, P.C., Mar. 2015. Spontaneous fractures in custom-made porous hydroxyapatite cranioplasty implants: is fragility the only culprit? Acta Neurochir. 157 (3), 517–523. https://doi.org/10.1007/s00701-014-2319-y.

Zanotti, B., Zingaretti, N., Verlicchi, A., Robiony, M., Alfieri, A., Parodi, P.C., Nov. 2016. Cranioplasty: review of materials. J. Craniofac. Surg. 27 (8), 2061. https://doi.org/10.1097/SCS.0000000000003025.

OssDsign 510 (K161090) [Online]. Available: https://www.fda.gov. (Accessed 24 July 2019).